Physicochemical stability of high indomethacin payload ordered mesoporous silica MCM-41 and SBA-15 microparticles

Tarja Limnell [a,*,1], Teemu Heikkilä [b,f,1], Hélder A. Santos [a], Sanna Sistonen [a], Sanna Hellstén [c], Timo Laaksonen [a], Leena Peltonen [a], Narendra Kumar [d], Dmitry Yu. Murzin [d], Marjatta Louhi-Kultanen [c], Jarno Salonen [b], Jouni Hirvonen [a], Vesa-Pekka Lehto [e]

[a] Division of Pharmaceutical Technology, Faculty of Pharmacy, University of Helsinki, FI-00014, Finland
[b] Laboratory of Industrial Physics, Department of Physics and Astronomy, University of Turku, FI-20014, Finland
[c] Department of Chemical Technology, Lappeenranta University of Technology, FI-53851 Lappeenranta, Finland
[d] Laboratory of Industrial Chemistry, Process Chemistry Centre, Åbo Akademi University, FI-20500 Turku, Finland
[e] Department of Physics, University of Kuopio, FI-70211, Finland
[f] Graduate School of Materials Research (GSMR), Turku, Finland

ARTICLE INFO

ABSTRACT

Stability of high indomethacin (IMC) content formulations based on ordered mesoporous silica MCM-41 and SBA-15 materials was studied before and after a 3 month storage in stressed conditions (30 °C/56% RH). Overall, the physical stability of the samples was found satisfactory after the storage. However, some issues with the chemical stability were noted, especially with the MCM-41 based samples. The stability issues were evident from the decreased HPLC loading degrees of the drug after stressing as well as from the observed extra peaks in the HPLC chromatograms of the drug in the stressed samples. Drug release from the mesoporous formulations before stressing was rapid at pH 1.2 in comparison to bulk crystalline IMC. The release profiles also remained similar after stressing. Even faster and close to complete IMC release was achieved when the pH was raised from 1.2 to 6.8. To our knowledge, this is the first report of chemical stability issues of drugs in mesoporous silica drug formulations. The present results encourage further study of the factors affecting the chemical stability of drugs in mesoporous silica MCM-41 and SBA-15 formulations in order to realize their potential in oral drug delivery.

© 2011 Elsevier B.V. All rights reserved.

1. Introduction

Administration of poorly water soluble drug compounds via the oral route is a growing challenge for the pharmaceutical industry. Poor solubility and/or permeability of a drug candidate in the intestinal lumen typically lead to unacceptable oral bioavailability. Due to the increasing complexity of new chemical entities, the problems of poor solubility are expected to worsen in the future. Thus, new drug solubility enhancing strategies are in demand.

Advancements in the use of ionic and non-ionic surfactants as structure directing agents led to the discovery of ordered mesoporous silica materials, MCM-41 and SBA-15 (Beck et al., 1992; Kresge et al., 1992; Zhao et al., 1998a,b). Therapeutic applications of

ordered mesoporous silica-based materials (i.e., porous materials with pore diameters of 2–50 nm) have been actively studied during the past decade. Numerous studies have been published where these novel inorganic materials are being developed towards medical applications, e.g. in the delivery of small molecule drugs and proteins, tissue engineering of multifunctional bone scaffolds, and intracellular vectors for stem cell tracking and gene transfection (Han et al., 1999; Vallet-Regí et al., 2001; Horcajada et al., 2004; Song et al., 2005; Vallet-Regí, 2006; Nunes et al., 2007; Suwalski et al., 2010). Notably, the mesoporous materials have shown potential for overcoming problems associated with the oral delivery of poorly soluble drug compounds. Formulations based on these materials could be used as solubility enhancing delivery platforms for a broad spectrum of drugs due to the high drug load capacity and inherent rapid drug release property (Heikkilä et al., 2007a,b; Van Speybroeck et al., 2009). Dissolution improvement is attained by incorporating a drug compound in the nanoscale pores of the mesoporous solid, where the confined space inhibits the crystallization of the entrapped drug molecules. This enables the delivery of the drug in its highly active amorphous form. As a proof-of-concept, an oral capsule formulation based on the ordered mesoporous silica

material SBA-15 has been shown to improve the bioavailability of poorly soluble antifungal drug itraconazole *in vivo* both in rabbits and dogs (Mellaerts et al., 2008).

Amorphous forms of drug compounds often show better solubility compared to their crystalline counterparts (Hancock, 2002). For example, the amorphization of indomethacin (IMC) improves its water solubility at room temperature by a factor of 4.5 (Hancock and Parks, 2000), and a notable increase in the initial dissolution rate has also been shown (Imaizumi et al., 1980; Savolainen et al., 2009). However, pure amorphous IMC typically recrystallizes in days if stored at ambient conditions (Yoshioka et al., 1994). It is evident that a delivery system that would stabilize the disordered form of the drug, but still enable fast and steady release kinetics, would be highly desirable for IMC. Such properties have been previously shown for ordered mesoporous silica materials MCM-41 and SBA-15 loaded with ibuprofen and IMC (Vallet-Regí et al., 2001; Heikkilä et al., 2007b; Van Speybroeck et al., 2009). Related mesoporous material, oxidized mesoporous silicon (PSi) has been shown to stabilize the disordered IMC under the stressed conditions (40 °C/75% RH) up to 6 months (Wang et al., 2010). Oxidized PSi also facilitated an improvement in the IMC dissolution profile *in vitro* (pH 7.2), as well as in the bioavailability in rats *in vivo*, even when compared to commercial IMC formulation (Indocid®). However, the IMC concentration in the oxidized-PSi microparticles was very low (~5.6 wt.-%). Rapid IMC release has also been observed in the case of SBA-15 carrier with IMC payload of 18.5 wt.-% (Van Speybroeck et al., 2009). In this case, the release rate was also maintained after 6 months of storage at 25 °C/52% RH.

IMC is a widely studied poorly soluble drug with challenging physicochemical properties (Table 1). In the present study, we have prepared high IMC-content samples with ordered mesoporous silica materials MCM-41 and SBA-15. Obtaining and studying samples with as high payloads as possible is important considering that the size of the eventual tablet formulation is limited. Also, the cost of the production of the ordered mesoporous silica carrier for the final formulation will be lower if the payload capacity can be fully utilized, i.e. the pores are totally filled with the active drug compound. As with any new combination of drug and excipient, the study of the physicochemical stability of the drug/silica compositions is essential to enable their further development towards actual formulations. So far only few studies on the aging behaviour of drug formulations based on mesoporous silica have been published (Van Speybroeck et al., 2009; Mellaerts et al., 2010; Shen et al., 2010). Here, we focused on the study of the physical and chemical stability of high IMC content MCM-41 and SBA-15 samples before and after 3 months stressing at 30 °C and 56% RH. The drug loading and release behaviour between the two mesoporous silica materials and their two particle size fractions was also compared.

2. Materials and methods

2.1. Synthesis of ordered mesoporous silica MCM-41

Synthesis of the mesoporous MCM-41 material was carried out in a 300 ml autoclave as described elsewhere (Heikkilä et al., 2010). The reagents used in the synthesis were fumed silica (SiO_2, 99.9%), tetramethylammonium silicate ((CH_3)$_4$N(OH)·$2SiO_2$, 99.99%), sodium silicate ($Na_2O_7Si_3$, SiO_2, 27%), cetyltrimethylammonium bromide (CTAB, $CH_3(CH_2)_{15}N(CH_3)_3Br$, 99%) (all from Sigma–Aldrich, St. Louis, MO, USA) and distilled water. A gel mixture was prepared and introduced in a Teflon cup, which was inserted in a 300 ml autoclave. The autoclave was kept in a large oven and the synthesis of MCM-41 was performed at 100 °C. After the completion of synthesis, the autoclave was taken out of the oven and quenched. Mesoporous silica MCM-41 was filtered and

washed with distilled water. Drying of the sample was carried out at 110 °C for 12 h and calcinated at 550 °C for 10 h.

2.2. Synthesis of ordered mesoporous silica SBA-15

Synthesis of the mesoporous SBA-15 material was performed in a 300 ml autoclave as described elsewhere (Heikkilä et al., 2010). The reagents used in the synthesis were Pluronic P123 co-block polymer (BASF, Ludwigshafen, Germany), HCl (33–40%, J.T. Baker, Phillipsburg, NJ, USA), tetraethyl orthosilicate (TEOS, $Si(OC_2H_5)_4$, 98%, Sigma–Aldrich, St. Louis, MO, USA) and distilled water. The prepared gel was introduced in a Teflon cup and inserted into a 300 ml autoclave. The autoclave was then kept in a large oven heated at 100 °C. The synthesis of SBA-15 was carried out at 100 °C for 24 h. After completion of the synthesis, the mesoporous silica was filtered and washed with 1000 ml of distilled water, dried at 100 °C for 12 h and calcinated at 500 °C for 7 h.
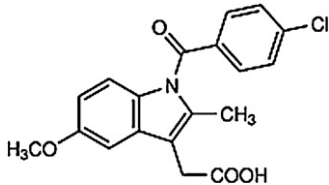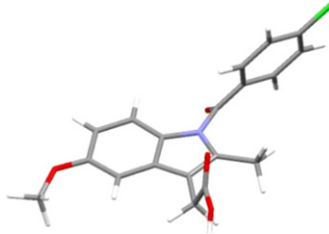
2.3. Preparation of indomethacin (IMC) samples

γ-IMC (USP grade) was purchased from Hawkins Inc. (Minneapolis, MN, USA) and passed through a mesh 500 (25 μm) test sieve (Retsch, Haan, Germany) before use. The sieved γ-IMC was designated as sample γ-IMC/25. α-IMC was prepared with the anti-solvent precipitation method described elsewhere (Kaneniwa et al., 1985) by adding distilled water in saturated solution of IMC in hot ethanol (EtOH, 99.6%, Altia Oyj, Helsinki, Finland). The sample was designated as α-IMC. The purchased and processed IMC samples were stored in ambient conditions protected from light. The presence of γ- and α-IMC phases were confirmed with powder X-ray diffraction (XRD) by comparing the measured and calculated patterns based on the structural data published in the CSD (Cambridge Structural Database; Allen, 2002) for the corresponding phases (INDMET02 and INDMET03).

2.4. Preparation of indomethacin (IMC)-loaded mesoporous silica samples

The synthesized mesoporous silica material MCM-41 was ground using a ball mill and the resulting fine powder was passed through a mesh number 230 (63 μm) test sieve using a sieve shaker apparatus (Fritsch GmbH, Idar-Oberstein, Germany). The sieved silica powder was then collected from the bottom pan and designated as sample MCM/1. The second sample of MCM-41 powder, designated as MCM/2, was prepared by sieving the silica powder through a mesh number 120 (125 μm) test sieve. Similarly, two samples of sieved silica SBA-15 powder were prepared and labelled as SBA/1 and SBA/2. IMC was loaded in the mesoporous silica samples MCM/1 and MCM/2 using an immersion method (Heikkilä et al., 2007b; Limnell et al., 2011). First a high concentration (250 mg/ml) of IMC solution was prepared by dissolving 750 mg of γ-IMC in 3 ml of hot EtOH (68 ± 2 °C). Then 150 mg of silica was added in the solution and gently mixed on a magnetic stirrer for 1 h. The silica particles were separated from the solution by vacuum filtration through a Versapor-1200 membrane disc filter (Pall Corporation, East Hills, NY, USA) with a 1.2 μm pore size. The filtrated silica particles were dried on the filter for 24 h at 65 °C and then collected for use. The IMC-loaded MCM-41 silicas were labelled as samples MCM/1/IMC and MCM/2/IMC. Similarly, the mesoporous silica samples SBA/1 and SBA/2 were loaded using the immersion method, except that the concentration of the IMC solution was slightly lower (180 mg/ml), prepared by dissolving 540 mg of γ-IMC in 3 ml of hot EtOH (68 ± 2 °C). The IMC-loaded SBA-15 particles were labelled as samples SBA/1/IMC and SBA/2/IMC.

Table 1
Physicochemical properties of IMC.

Structure	
Therapeutic class	Non steroidal anti-inflammatory drug (NSAID)
Formula	$C_{19}H_{16}ClNO_4$
Molecule dimensions[a]	1.36 nm × 0.82 nm × 0.56 nm
Molecular weight	357.79 g/mol
Polymorphism and solvates	Two main polymorphs (α and γ) and capable of forming solvates (Kaneniwa et al., 1985)
pK_a	4.5 (Avdeef, 2001)

	α-form	γ-form
Melting point	153 °C (Legendre and Feutelais, 2004)	159 °C (Legendre and Feutelais, 2004)
Solubility	9 µg/ml (35 °C, water) (Kaneniwa et al., 1985)	7 µg/ml (35 °C, water) (Kaneniwa et al., 1985)
	13 µg/ml (45 °C, water) (Hancock and Parks, 2000)	10 µg/ml (45 °C, water) (Hancock and Parks, 2000)
		10 µg/ml (pH 7.2 in PBS, RT) (Savolainen et al., 2009)
		784 µg/ml (37 °C, pH 6.8) (Patterson et al., 2005)

[a] Longest dimensions (x, y, z) determined using Mercury 2.3 (CCDC, 2009) software and molecule data downloaded from DrugBank (www.drugbank.ca).

2.5. Stressing of the samples

The silica/IMC samples were stored at elevated conditions of temperature and relative humidity for the study of the physicochemical stability and aging behaviour. The samples were first characterized as prepared, and then placed in a desiccator with a saturated salt solution of sodium bromide (NaBr) producing a relative humidity atmosphere of 56% RH. The desiccator was placed in an oven at 30 °C. The samples were protected from light. The storage period was 3 months, after which the stressed silica/IMC samples were characterized again. The stressed samples were designated as MCM/1/IMC/S and MCM/2/IMC/S for MCM-41 materials, and SBA/1/IMC/S and SBA/2/IMC/S for SBA-15 materials.

2.6. Physical characterization

The crystallinity and structural properties of the samples were characterized with XRD using nickel filtered Cu Kα (λ = 1.542 Å) radiation operated at 40 kV/50 mA (PANalytical, Almelo, The Netherlands). Thermogravimetric (TG) analysis was performed on a TGA-7 instrument (PerkinElmer, Waltham, MA, USA) with a heating rate of 10 °C/min under a N_2 gas purge of 40 ml/min. Alumel, nickel, perkalloy and iron were used to calibrate the TG temperature scale. The differential scanning calorimetry (DSC) analysis was carried out with a Pyris Diamond DSC (PerkinElmer, Waltham, MA, USA) using a heating rate of 20 °C/min under a N_2 gas purge of 40 ml/min in 30 µl aluminium sample pans with pierced lids. Indium was used to calibrate the temperature and heat flow scales. The TG and DSC measurements were performed in triplicate (n = 3). The porous properties of the microparticles were characterized with N_2 adsorption/desorption measurements on a Tristar 3000 (Micromeritics, Norcross, GA, USA) instrument at −196 °C. The pure silica particles were evacuated at 250 °C for 24 h preceding the measurements using a VacPrep (Micromeritics, Norcross, GA, USA) degasser. The IMC-loaded particles were evacuated at room temperature for 24 h preceding the measurements. The surface areas and pore characteristics were determined by the BET (Brunauer–Emmett–Teller; Brunauer et al., 1938) and BJH (Barrett–Joyner–Halenda; Barrett et al., 1951) methods. The particle size distributions were measured with a Mastersizer 2000 (Malvern, Worcestershire, UK) laser diffraction instrument equipped with a Hydro 2000G wet dispersion sampler. Water was used as the dispersant with the pump and stirrer speeds of 2500 and 1000 rpm, respectively. Scanning electron microscopy (SEM) was performed on a S200 SEM (Cambridge, Cambridge, UK). The samples were sputter coated with gold prior to imaging. The attenuated total reflectance (ATR)-Fourier transformed infrared (FTIR) spectroscopy analysis was conducted on Spectrum BX FTIR Spectrometer (PerkinElmer, Waltham, MA, USA) equipped with a MIRacle single reflection ATR sampling accessory with a diamond/ZnSe crystal plate (Pike Technologies, Madison, WI, USA). For each ATR-FTIR spectra 100 scans were collected. The solid state of the non-stressed samples was characterized with Jobin-Yvon LabRam 300 Raman microscope (HORIBA, Ltd., Kyoto, Japan) equipped with a liquid nitrogen cooled CCD detector and an external cavity stabilized single mode diode laser at 785 nm. Raman spectra were captured with the confocal hole set to 1000 µm and the slit width to 100 µm using an acquisition time of 15 s with two accumulations. Partial least squares (PLS) regression with principal component analysis (PCA) was utilized to obtain information on the distribution of the different solid forms (Heinz et al., 2007).

2.7. Drug release experiments

The dissolution experiments were performed using a USP dissolution paddle method at 100 rpm (Erweka DT-D6, Heusenstamm, Germany). The buffer solution used was 500 ml of 0.2 M HCl/KCl (pH 1.2) at +37 °C. In the experiments including the pH change from 1.2

to 6.8 0.1 M HCl was used as the initial medium at pH 1.2, which was further raised to pH 6.8 by adding 141 ml of 0.2 M Na_3PO_4 at +37 °C after 30 min of dissolution. The silica/IMC samples were weighed directly into hard gelatine capsules. The target was 200 μg of IMC in the capsules. The weighed amount of silica/IMC was adjusted based on the total IMC payload determined by TG analysis. A small magnet was used as a sinker in each capsule to ensure proper wetting of the samples. All the experiments were performed at least in triplicate ($n = 3–4$) over 60 min and under sink conditions, i.e. the volume of the medium was at least three times greater than that required to form a saturated solution of the studied drug substance. During the dissolution experiments, aliquots of 0.5 ml were collected at certain time intervals for posterior IMC quantification by HPLC. The sample volume was not supplemented as the change in the overall volume was small. After the last sampling, the silica particles were filtered from the dissolution medium and incubated in 2 ml of EtOH for 24 h (room temperature) in order to release the remaining IMC from the particles. The sum of IMC released by the samples during the dissolution experiments and in the EtOH incubation was considered as the total amount of drug released (100%) in each experiment, except for the pH change experiments, where no EtOH incubation was performed due to the almost complete release of IMC from the pores at pH 6.8.

2.8. IMC quantification and purity evaluation by HPLC

The total IMC-content in the MCM-41 and SBA-15 silica particles before and after stressing was quantified by HPLC. Samples of 0.5–1 mg of the loaded particles were weighed into a half of a gelatine capsule and added to a mixture of pure water and EtOH (50:50, v/v). The mixture was vigorously stirred overnight. The samples were then filtered and analyzed by HPLC. IMC concentrations in the samples were determined by HPLC (Agilent 1100 Series, Agilent Technologies, Waldbronn, Germany) using an Agilent G1365B Multiple Wavelength Detector, an Agilent G1367A Well-Plate Autosampler, an Agilent G1316A Thermostatted Column Compartment (at +25 °C), an Agilent G1312A Binary pump and an Agilent G1379A Micro Vacuum Degasser. The mobile phase during determination ($λ = 320$ nm, retention time ∼4.1 min) consisted of acetonitrile and 0.2% phosphoric acid pH 2.0 (60:40). A Luna 100 Å C18 reversed-phase column (150 × 4.6 mm; 3 μm) with a C18 guard column 4 × 30 mm (Phenomenex, Torrance, CA, USA) was used at a flow rate of 1.5 ml/min. Volumes of 20 μl were injected for the analyses.

The purity evaluation was performed by calculating the relative area of the possible degradation peak compared to the corresponding IMC peak. The achieved relative values between non-stressed and stressed samples were then compared.

3. Results

The XRD patterns of MCM/1, MCM/2, SBA/1, and SBA/2 showed well resolved $h k l(1 0 0)$, $h k l(1 1 0)$, $h k l(2 0 0)$ and $h k l(2 1 0)$ peaks, characteristic for the corresponding mesoporous silica materials with hexagonal unidirectional mesopore systems (Fig. 1) (Beck et al., 1992; Kresge et al., 1992; Zhao et al., 1998a,b). The XRD data was supplemented by the N_2 sorption measurements (Fig. 2). The N_2 sorption isotherms were typical type-IV according to the IUPAC classification, with the inflections of the capillary condensation observed (Sing et al., 1985). All samples were clearly mesoporous as shown by the N_2 adsorption/desorption results in Table 2. Results for particle size (laser diffraction measurements) and shape (SEM imaging) are presented in Table 2.

The IMC loading solution concentrations were selected so that the loaded drug amount would be as high as possible, while keeping
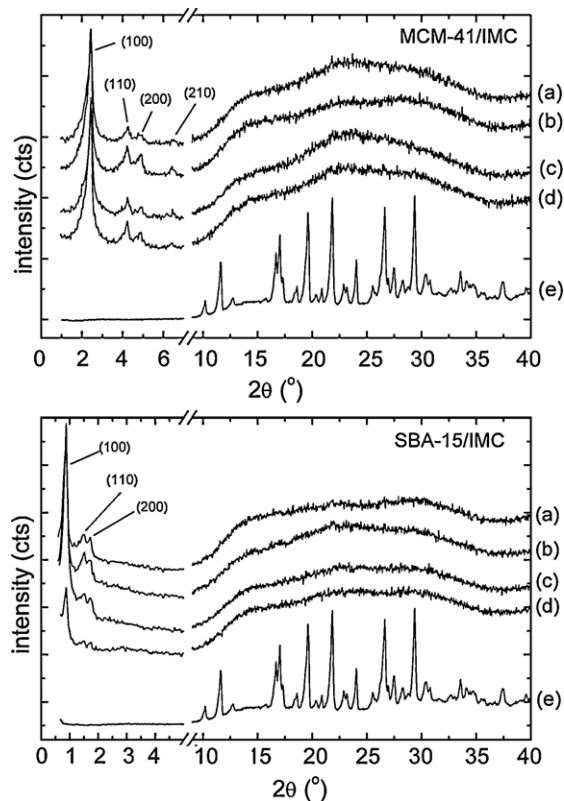

Fig. 1. XRD patterns for the MCM-41 samples: (a) MCM/2/IMC/S, (b) MCM/2/IMC, (c) MCM/1/IMC/S, (d) MCM/1/IMC and (e) γ-IMC/25 for comparison in the top figure. In the bottom figure the XRD patterns for the SBA-15 samples: (a) SBA/2/IMC/S, (b) SBA/2/IMC, (c) SBA/1/IMC/S, (d) SBA/1/IMC and (e) γ-IMC/25 for comparison.

the crystalline content very low. The produced silica/IMC samples had a high payload of IMC as shown by TG, with a maximum IMC-content of 39.3 wt.-% ($w_{IMC}/w_{IMC+silica}$), i.e. 65% (w_{IMC}/w_{silica}) in SBA/2/IMC (Table 3, Fig. 3). Residual EtOH was not detected by FTIR in the studied samples (Fig. 4). N_2 sorption exhibited a dramatic decrease of the particle pore volume in both silicas due to the inclusion of high amounts of IMC; for example, from 0.785 to 0.136 cm^3/g for empty MCM/1 and loaded MCM/1/IMC, respectively (Table 2). Varied, although minor (<3.0 wt.-%), amounts of crystalline IMC were detected by DSC in the samples directly after loading (Table 3, Fig. 5). Raman spectroscopy was also used to characterize in more detail the solid form of IMC crystallized on the surface of the particles. Raman mapping revealed that the particle surfaces were partly covered with a mixed γ/α-IMC phase. The crystalline γ/α-IMC was distributed evenly on the surface of the mesoporous particles, i.e. no large clusters of crystalline IMC were observed before stressing (distribution maps not shown). In all of the samples, the surfaces had a slightly higher relative amount of γ-IMC in comparison to the α-IMC (Table 3).

No significant changes were observed in the ATR-FTIR spectra of the samples before and after storage (Fig. 4). N_2 sorption analysis showed only minor decrease in the free pore volume of the silica/IMC particles after the stressing period, indicating stable inclusion of the drug in the mesoporous materials (Table 2). DSC analysis showed that the melting temperatures of the crystalline IMC solid forms on the surface of the silica particles were somewhat lower after storage (Table 3). Decrease in the melting enthalpies was also detected in the MCM-41 samples. Thus, the amount of crystalline IMC calculated from the melting enthalpies seemed to have slightly decreased in the MCM-41 samples during storage, but not in the SBA-15 samples. Less pure compounds typically show a lower melting temperature and wider melting
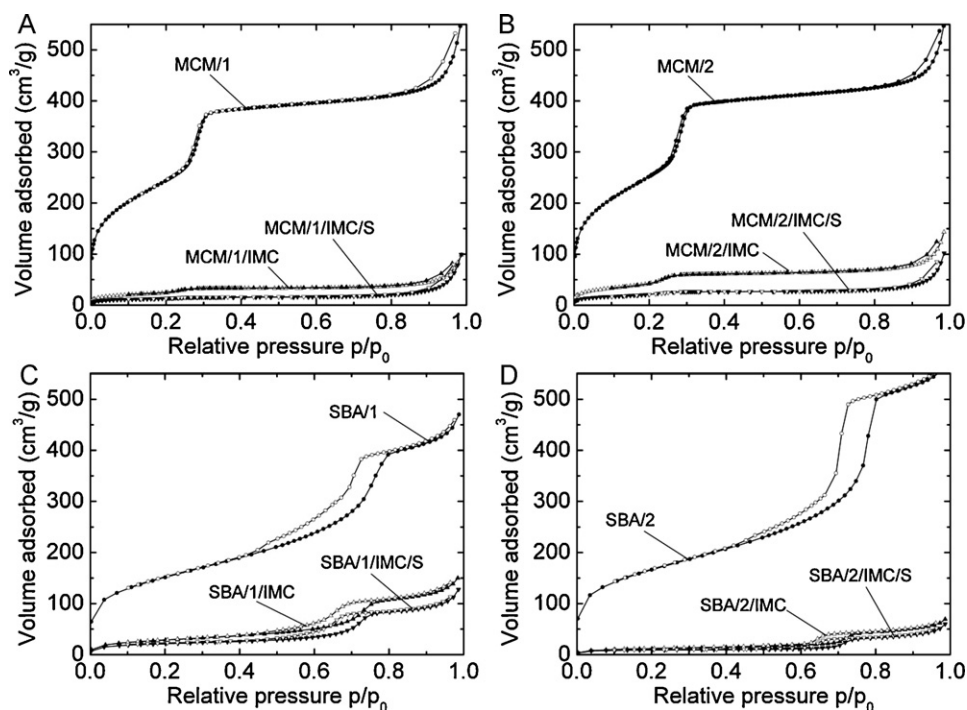
Fig. 2. Nitrogen adsorption/desorption isotherms for (A) MCM/1, MCM/1/IMC, MCM/1/IMC/S, (B) MCM/2, MCM/2/IMC, MCM/2/IMC/S, (C) SBA/1, SBA/1/IMC, SBA/1/IMC/S and (D) SBA/2, SBA/2/IMC, SBA/2/IMC/S samples. The adsorption and desorption isotherms are marked with closed and open symbols, respectively.

endotherm in comparison to pure compounds. Hence the depression of the melting point and decreased melting enthalpy seen in the present study may be a sign of lower purity of IMC after stressing.

The HPLC measurements showed that the produced silica/IMC samples had a high payload of IMC with a maximum IMC-content of 40.9 wt.-% ($w_{IMC}/w_{IMC+silica}$) in SBA/2/IMC (Table 3). The high payload of SBA-15 samples remained unchanged after stressing. A decrease from 30.9 to 22.8 wt.-% and from 31.9 to 21.7 wt.-% was revealed in the IMC-content of the MCM/1/IMC and MCM/2/IMC particles, respectively, after stressing (Table 3). The observation was supported by the DSC melting results discussed above, as well as the HPLC chromatograms, where increase in possible IMC degradation peaks at relative retention times (RRTs) of 0.7 and 1.8 were seen after the stressing (Fig. 6). The change was more evident for MCM-41 than for SBA-15 samples. For example, the peak in MCM/1/IMC/S at RRT

of 1.8 was 9.82 times larger than in the non-stressed sample, while the corresponding value for SBA/1/IMC/S was 2.67 (Table 4). The HPLC and TG payload results were in good agreement, except for the stressed MCM-41 samples, where TG detected no changes in the IMC-content of the samples before and after stressing, in contrast to the HPLC results (Table 3).

Drug release from the mesoporous silica particles was improved as compared to the reference γ-IMC/25 (Fig. 7). The IMC release from SBA/1/IMC and SBA/2/IMC was fast in the beginning and slowed down after 15–20 min, while the corresponding IMC release from MCM/1/IMC and MCM/2/IMC was slower and continued through the whole 60 min experiment. After stressing, the IMC release seemed to be somewhat slower from all formulations, while the release profiles remained similar. Drug release close to 100% was achieved when the pH of the dissolution medium was raised from 1.2 to 6.8 (Fig. 8).

Table 2
Particle size, shape and porous characteristics of the silica samples.

Sample	Particle shape[a]	D_v90 (μm)[b]	D_v50 (μm)[c]	D_{BJH} (nm)[d]	S_{BET} (m²/g)[e]	V_p (cm³/g)[f]
MCM/1	Modular	72.4	36.1	2.5	909	0.785
MCM/1/IMC				2.2	86	0.136
MCM/1/IMC/S				2.2	47	0.136
MCM/2	Granular	161.3	78.0	2.5	935	0.789
MCM/2/IMC				2.2	152	0.199
MCM/2/IMC/S				2.2	74	0.142
SBA/1	Modular	54.0	22.4	7.9	535	0.709
SBA/1/IMC				6.9	102	0.234
SBA/1/IMC/S				6.9	76	0.179
SBA/2	Acicular	117.4	26.9	8.3	597	0.880
SBA/2/IMC				6.7	41	0.103
SBA/2/IMC/S				6.7	31	0.088

[a] Predominant particle shape in the samples evaluated by SEM imaging.
[b] Laser diffraction particle of undersize volume 90%.
[c] Laser diffraction particle of undersize volume 50%.
[d] Peak value of the BJH pore size distribution.
[e] BET surface area.
[f] BJH total pore volume.

Table 3
Drug load and crystallinity characteristics of the samples before and after 3 month storage at 30 °C/56% RH. Samples that were stored under stressed conditions are denoted with /S.

Sample	IMC$_{HPLC}$ (wt.-%)[a]	IMC$_{TG}$ (wt.-%)[b]	t_m (°C)[c]	ΔH (J/g)[d]	IMC$_{cryst}$ (wt.-%)[e]	γ/α/amorphous IMC (%)[f]
MCM/1/IMC	30.9 ± 0.5	28.5 ± 1.5	157.1 ± 0.1	2.2 ± 0.6	2.1 ± 0.6	30/26/44
MCM/1/IMC/S	22.8 ± 2.0	28.2 ± 1.4	156.3 ± 0.4	0.8 ± 0.3	0.7 ± 0.3	–
MCM/2/IMC	31.9 ± 0.5	28.5 ± 2.1	157.2 ± 0.3	1.9 ± 0.8	1.8 ± 0.8	30/26/44
MCM/2/IMC/S	21.7 ± 0.9	27.6 ± 1.7	156.6 ± 0.4	0.5 ± 0.3	0.5 ± 0.3	–
SBA/1/IMC	29.5 ± 1.0	27.1 ± 0.7	151.6 ± 0.2	3.1 ± 0.6	3.0 ± 0.6	34/33/33
SBA/1/IMC/S	32.7 ± 5.4	27.5 ± 1.0	151.2 ± 0.2	3.5 ± 2.6	3.4 ± 2.6	–
SBA/2/IMC	40.9 ± 1.3	39.3 ± 1.0	156.9 ± 0.6	0.4 ± 0.6	0.3 ± 0.6	33/29/38
SBA/2/IMC/S	38.5 ± 4.2	38.5 ± 0.8	155.5 ± 0.3	0.3 ± 0.5	0.3 ± 0.5	–
γ-IMC/25[g]	100.0	100.0	159.1 ± 0.1	106.0 ± 0.9	100	100/0/0
α-IMC[h]	n/m	100.0	152.9 ± 0.1	101.0 ± 0.9	100	9/91/0

[a] Total IMC-content as weight$_{IMC}$/weight$_{IMC+silica}$ (HPLC).
[b] Total IMC-content as weight$_{IMC}$/weight$_{IMC+silica}$ (TG).
[c] Melting temperature onset for the crystalline IMC in the samples (DSC).
[d] Melting enthalpy of crystalline IMC the samples (DSC).
[e] Amount of crystalline IMC in sample calculated from the DSC melting endotherm data: area$_{peak,endotherm}$(mJ)/$\Delta H_{enthalpy,pure\ γ/α-IMC}$(J/g) × mass$_{sample,DSC}$ (mg).
[f] Raman mapping quantification of the crystalline IMC phases on the sample surfaces.
[g] γ-IMC, passed through a mesh 500 sieve (25 μm).
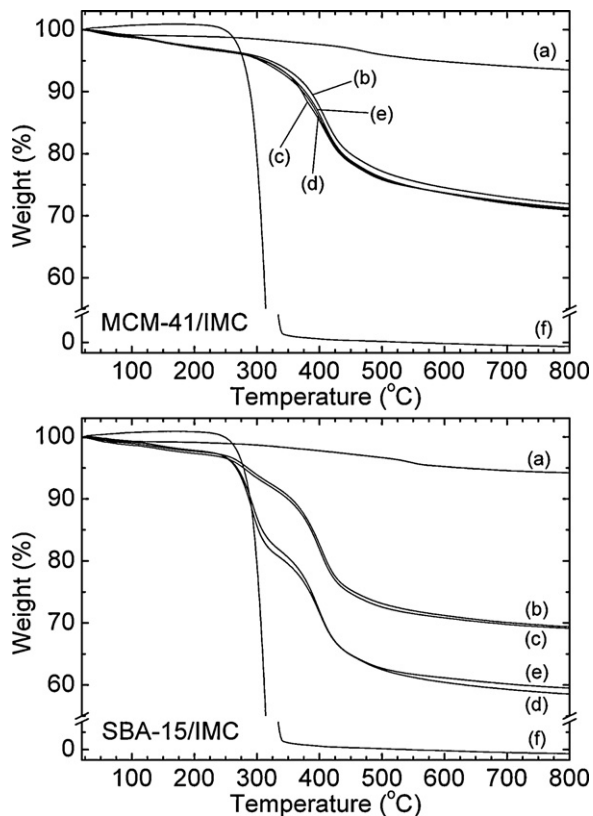[h] α-IMC, crystallized from an EtOH/water solution.

Fig. 3. Representative TG curves ($n = 3$). In the top figure for MCM-41/IMC samples: (a) MCM/1, (b) MCM/2/IMC/S, (c) MCM/2/IMC, (d) MCM/1/IMC, (e) MCM/1/IMC/S, and (f) γ-IMC/25 for comparison. In the bottom figure for SBA-15/IMC samples: (a) SBA/1, (b) SBA/1/IMC, (c) SBA/1/IMC/S, (d) SBA/2/IMC/S, (e) SBA/2/IMC and (f) γ-IMC/25 for comparison.

Fig. 4. ATR-FTIR spectra. In the top figure the spectra for the MCM-41 samples: (a) γ-IMC/25, (b) MCM/1, (c) MCM/1/IMC, (d) MCM/1/IMC/S, (e) MCM/2, (f) MCM/2/IMC, (g) MCM/2/IMC/S and for comparison (h) MCM/2/IMC moistured in EtOH. In the bottom figure the spectra for the SBA-15 samples: (a) γ-IMC/25, (b) SBA/1, (c) SBA/1/IMC, (d) SBA/1/IMC/S, (e) SBA/2, (f) SBA/2/IMC, (g) SBA/2/IMC/S and for comparison (h) SBA/2/IMC moistured in EtOH.

4. Discussion

The much higher surface areas of the MCM-41 carriers (MCM/1 and MCM/2, >900 m²/g) did not enable a higher drug load in comparison to the SBA-15 carrier with lower surface area (SBA/1, 535 m²/g). We found that the most important physical parameter of the mesoporous silica for achieving high load efficiency was the pore volume (SBA/2, 0.880 cm³/g). The particle size fraction was
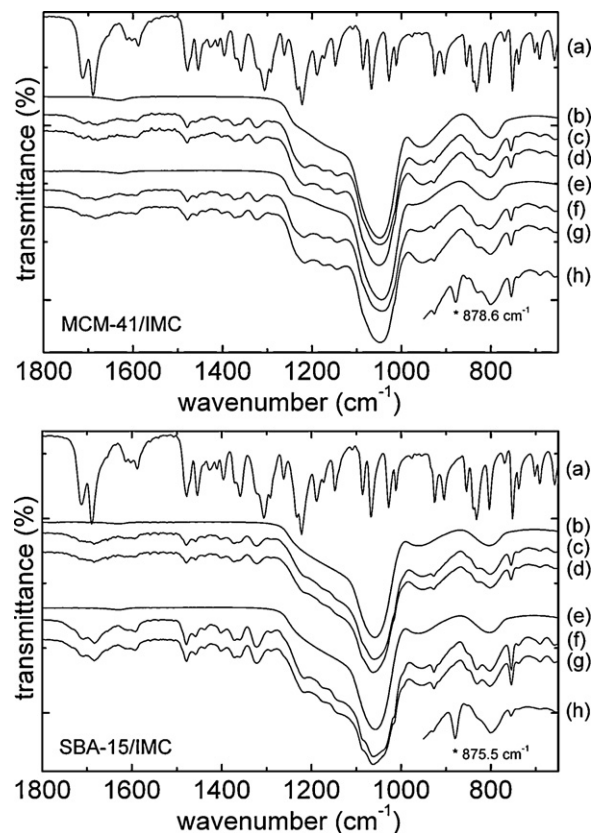
not found to have a major effect on the drug load or the amount of drug crystallized on the surface of particle, at the tested size range.

There were no major changes in the physical properties (crystallinity and porous characteristics) of the samples before and after stressing. The mesoporous silica carriers stabilized the amorphous state of IMC for at least the storage period of 3 months (at 30 °C/56% RH), whereas amorphous IMC (produced by rapid melt quenching)
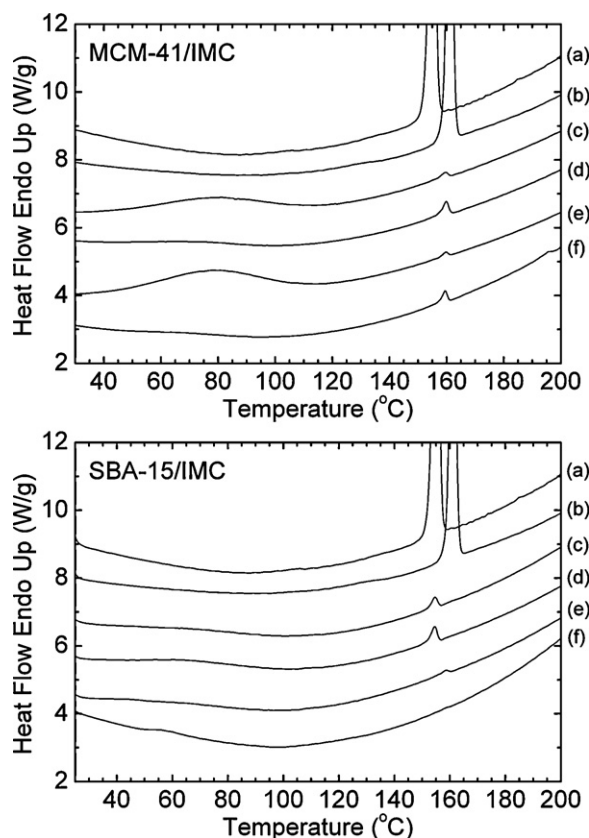
Fig. 5. Representative DSC thermograms (*n* = 3). In the top figure the DSC thermograms for MCM-41/IMC samples: (a) α-IMC (crystallized from EtOH/water solution), (b) γ-IMC/25, (c) MCM/1/IMC/S, (d) MCM/1/IMC, (e) MCM/2/IMC/S and (f) MCM/2/IMC. In the bottom figure the DSC thermograms for SBA-15/IMC samples: (a) α-IMC, (b) γ-IMC/25, (c) SBA/1/IMC/S, (d) SBA/1/IMC, (e) SBA/2/IMC/S and (f) SBA/2/IMC.

Table 4
Comparisons between the relative peak areas of the possible IMC degradation peaks of the stressed particles at RRTs of 0.7 and 1.8 (mean ± SD, *n* = 2) and the corresponding peaks in non-stressed particles with a reference value of 1.00. The representative HPLC chromatograms of the samples are shown in Fig. 6.

Sample	RRT 0.7	RRT 1.8
MCM/1/IMC/S	4.58 ± 0.2	9.82 ± 7.9
MCM/2/IMC/S	5.23 ± 1.4	12.78 ± 3.1
SBA/1/IMC/S	2.05 ± 0.4	2.67 ± 0.1
SBA/2/IMC/S	0.80 ± 0.5	2.80 ± 1.6

without any stabilizer has been reported to crystallize already in 2 days at 30 °C (Crowley and Zografi, 2003).

There were issues with the chemical stability of the IMC payloads as shown by the HPLC measurements (Fig. 6, Table 3). This was especially evident for the MCM-41 samples, where a clear decrease in the active IMC-content was detected. TG showed no significant changes in the sample mass before and after stressing, which indicated that both the active and degraded IMC remained in the particles due to the mesopore inclusion. Emerging degradation products may, on the other hand, contribute to the observed slight decrease in the surface IMC melting temperatures, especially with MCM-41 (Table 3). The main route of degradation of IMC is the breakage of the amide linkage leading to two different substructures: 4-chlorobenzoic acid and 5-methoxy-2-methylindoleacetic acid (Nováková et al., 2005). Other possible impurities have also been recognized, such as oxidation products and synthesis derived esters (Hess et al., 2001; Li et al., 2005). In our studies, the major possible degradation products eluted at RRTs of 0.7 and 1.8. As the HPLC method was not optimized for the degradation product quantification, the evaluations were made based on relative peak areas between the IMC degradation product peaks and the corresponding IMC peak. These values were then compared between non-stressed and stressed samples. The peak of the IMC degradation product at RRT 0.7 overlaps with the peak from EtOH used in extracting of the samples. This explains its presence already in the chromatograms of the non-stressed samples. The RRT 1.8 peak could also be detected in the non-stressed samples. The extra peaks in the chromatograms could at least partly explain the decrease and deviation in the HPLC-determined IMC-loading degree results before and after stressing. The structural studies of the IMC degradation products are out of
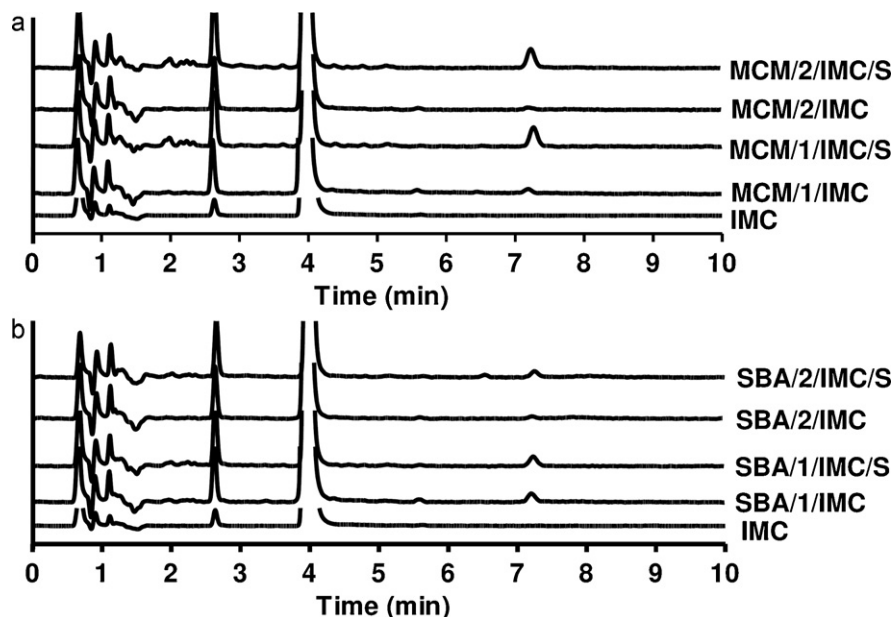

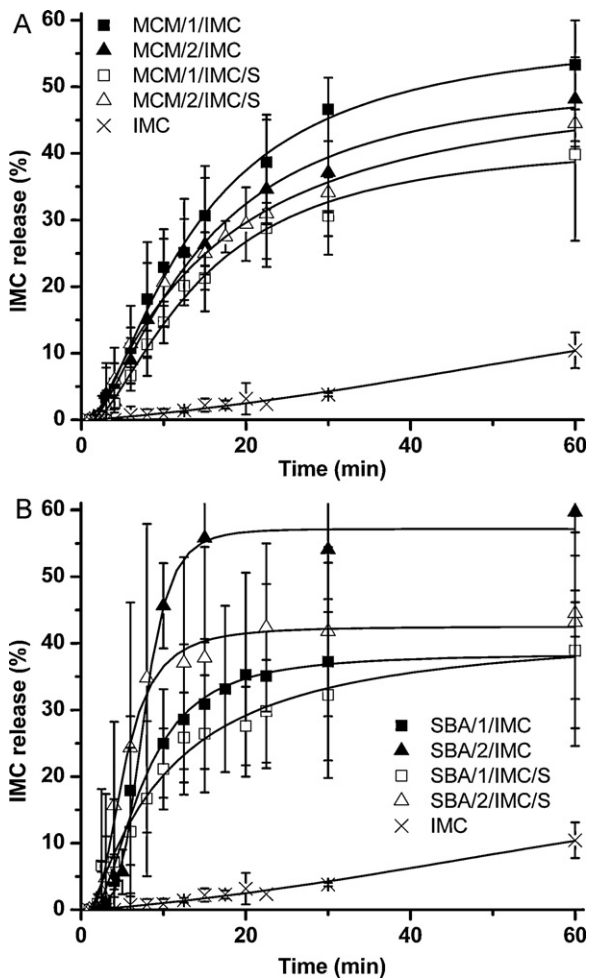**Fig. 6.** HPLC chromatograms for MCM-41 (A) and SBA-15 (B) based samples.

Fig. 7. Dissolution profiles of IMC released from encapsulated MCM-41 (A) and SBA-15 (B) based samples ($n = 3$–4, mean ± SD). The dissolution medium used was 0.2 M HCl/KCl (pH 1.2) at +37 °C. Bulk IMC is included as a reference. Lines are a guide to the eye only.

scope of this study, and thus, the total amount or structure of the degradation products were not further determined. In the future, this could be addressed, e.g. by performing nuclear magnetic resonance (NMR) or liquid chromatography–mass spectrometry
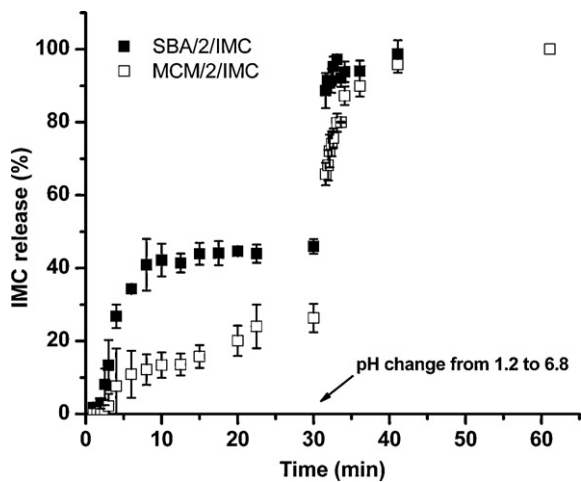

Fig. 8. Dissolution profiles of IMC released from encapsulated MCM-41 and SBA-15 based samples ($n = 3$, mean ± SD). Dissolution medium was 0.1 M HCl at pH 1.2 which was further raised to pH 6.8 by adding 0.2 M Na$_3$PO$_4$ at +37 °C after 30 min of dissolution.

(LC–MS) studies for evaluating the structural changes in the drug molecules (Babonneau et al., 2004; Hess et al., 2001; Li et al., 2005). In addition, NMR studies can also give an insight into the possible interactions between the drug and the silica surface (Babonneau et al., 2003, 2004; Watanabe et al., 2001). It is known that the silanol groups on the surfaces of silica may interact with the carboxyl and benzoyl carbonyl groups of IMC and stabilize its amorphous form (Bahl and Bogner, 2006). The number of silanol groups/nm^2, α_{OH}, on the silica surface varies between different silica materials and is also affected by the post-synthetic treatments of the material (Kozlova and Kirik, 2010). Despite slight variation in the exact values of different studies, the number of silanol groups per area unit is generally higher in SBA-15 (2.8–5.3 OH/nm^2) than in MCM-41 (1.4–3.0 OH/nm^2) silica materials (Zhao et al., 1997; Shenderovich et al., 2003; Kozlova and Kirik, 2010). Thus, even considering the surface area differences (Table 2) SBA-15 has more stabilizing groups available for interaction with IMC, which in turn may explain the observed better chemical stability of IMC in SBA-15 compared to MCM-41. Another reason behind the phenomenon may be the surface roughness of SBA-15 that is associated with Si(OH)$_2$ groups and is not present in MCM-41 (Shenderovich et al., 2003). The surface defects have been considered to be the reason for stronger hydrogen binding of water molecules into SBA-15 than into MCM-41. In theory, utilizing the same mechanism, the stabilization of IMC via hydrogen bonding could also be stronger in SBA-15 than in MCM-41 and induce better chemical stability.

The dissolution studies were performed in order to demonstrate the ability of both MCM-41 and SBA-15 microparticles to improve the dissolution of IMC by initially stabilizing it in a disordered state inside the mesopores and by further maintaining this state even during storage in stressed conditions. The dissolution media were chosen to emphasize the release differences between the formulations and to discriminate the possible changes in dissolution after stressing. The media also represent the harsh conditions of the stomach followed by the higher pH of the small intestine. MCM-41 has narrower pores than SBA-15 (Table 2), which has been proposed to contribute to a slower release rate due to steric hindrance that obstructs the diffusion of the drug molecules out of the pores (Qu et al., 2006; Cauda et al., 2009). This can be seen when comparing the IMC release from MCM-41 and SBA-15 (Fig. 7); the IMC release from the SBA-15 samples reaches the plateau faster, while the corresponding release profiles of the MCM-41 samples continue slowly through the whole experiment. The phenomenon is even more evident in the 0.1 M HCl solution (pH 1.2) (Fig. 8). The released drug amount remained at around the 40–60% level in the pH 1.2 buffer. Similar results at pH 1.2 have been previously reported for ibuprofen (pK_a = 5.6) (Charnay et al., 2004). Therefore, the incomplete dissolution for IMC (pK_a = 4.5) (Avdeef, 2001) was to be expected at this low pH. As the dissolution media were intentionally selected to be discriminating, small variations in the dissolution rate between different particle types were emphasized. When the release is faster, the differences between samples are less pronounced. Considering this, the observed slower release rate after stressing is not seen as such a major change in the behaviour of the materials that would affect their pharmaceutical performance. Assuming that a similar amount of IMC remains entrapped in the pores of the SBA-15 samples of similar surface areas due to surface interactions (Table 2), the higher level where the release from SBA/2/IMC reaches the slow release phase can be explained by the higher amount of IMC incorporated into those particles (for example, the loading degrees for SBA/1/IMC and SBA/2/IMC are 29.5 and 40.9%, respectively) (Kim et al., 2006). These results show a slower release than those reported with vigorous stirring using simulated gastric fluid without pepsin, supplemented with sodium lauryl sulfate, as a release medium (Van Speybroeck et al., 2009). The release of a drug from a particle is a sum of many different phenomena

including, for example, the effect of the larger pore diameter and the smaller particle size (Horcajada et al., 2004; Qu et al., 2006; Cauda et al., 2009), as well as density of the packing of the particles due to loading efficiency.

Close to complete (100%) release was observed with both MCM/2/IMC and SBA/2/IMC when the pH of the dissolution medium was raised from 1.2 to 6.8 after 30 min (Fig. 8). As a result of the pH raise, the remaining IMC fraction was released from the pores in only a few minutes. With this experiment, it was shown that the IMC indeed does completely come out of the pores in an aqueous environment and that the release can be controlled by the pH. When applied to the human gastrointestinal system, this kind of release behaviour could be beneficial and increase patient compliance. By loading a drug that is poorly soluble in acidic pH into mesoporous microparticles the pH dependence of the dissolution can be diminished and the drug can start dissolving already in the stomach (Salonen et al., 2005). In addition, if the drug has a potential to absorb already through the mucous membrane of the stomach or, alternatively, as the drug enters the duodenum faster in a solution than as solid, the onset of the clinical effect could also be achieved earlier (Collins et al., 1983). The remaining drug inside the pores would thus release only after the particles move through the pylorus to the more basic environment in the small intestine. Optimally, the drug release would be controlled, continuous and steady. The early onset of the absorption would be especially beneficial in the treatment of pain or for patients under continuous medication who are in need of a fast onset of treatment, for example, in the morning after a longer interval after the previous dose.

5. Conclusions

The physico-chemical stability of the high IMC payload samples based on ordered mesoporous silica materials, MCM-41 and SBA-15, during prolonged storage under stressed conditions was found to be variable. Although the physical stability of the samples was found satisfactory and the drug release performance was rapid after the storage, some impairment was observed in the chemical stability. The chemical analyses revealed a decrease in the loading degree and possible IMC degradation products formation, especially in MCM-41 based samples after stressing. Merely physical analyses or UV-detection of the drug release may not provide a full insight of the formulation stability. To our knowledge, this is the first report of chemical stability issues of drugs in mesoporous silica drug formulations. Therefore the factors affecting the chemical stability of drugs included in mesoporous silica carriers should be explored in more detail in the future.

Acknowledgements

References

Allen, F.H., 2002. The Cambridge Structural Database: a quarter of a million crystal structures and rising. Acta Crystallogr. B: Struct. Sci. 58, 380–388.

Avdeef, A., 2001. Physicochemical profiling (solubility, permeability and charge state). Curr. Top. Med. Chem. 1, 277–351.

Babonneau, F., Camus, L., Steunou, N., Ramila, A., Vallet-Regi, M., 2003. Encapsulation of ibuprofen in mesoporous silica: solid state NMR characterization. Mat. Res. Soc. Symp. Proc. 775, 77–82.

Babonneau, F., Yeung, L., Steunou, N., Gervais, C., Ramila, A., Vallet-Regi, M., 2004. Solid state NMR characterization of encapsulated molecules in mesoporous silica. J. Sol-Gel Sci. Technol. 31, 219–223.

Bahl, D., Bogner, R.H., 2006. Amorphization of indomethacin by co-grinding with neusilin US2: amorphization kinetics, physical stability and mechanism. Pharm. Res. 23, 2317–2325.

Barrett, E.P., Joyner, L.G., Halenda, P.P., 1951. The determination of pore volume and area distributions in porous substances. I. Computations from nitrogen isotherms. J. Am. Chem. Soc. 73, 373–380.

Beck, J.S., Vartuli, J.C., Roth, W.J., Leonowicz, M.E., Kresge, C.T., Schmitt, K.D., Chu, C.T.W., Olson, D.H., Sheppard, E.W., McCullen, S.B., Higgins, J.B., Schlenker, J.L., 1992. A new family of mesoporous molecular sieves prepared with liquid crystal templates. J. Am. Chem. Soc. 114, 10834–10843.

Brunauer, S., Emmett, P.H., Teller, E., 1938. Adsorption of gases in multimolecular layers. J. Am. Chem. Soc. 60, 309–319.

Cauda, V., Mühlstein, L., Onida, B., Bein, T., 2009. Tuning drug uptake and release rates through different morphologies and pore diameters of confined mesoporous silica. Micropor. Mesopor. Mater. 118, 435–442.

Charnay, C., Bégu, S., Tourné-Péteilh, C., Nicole, L., Lerner, D.A., Devoisselle, J.M., 2004. Inclusion of ibuprofen in mesoporous templated silica: drug loading and release property. Eur. J. Pharm. Biopharm. 57, 533–540.

Collins, P.J., Horowitz, M., Cook, D.J., Harding, P.E., Shearman, D.J., 1983. Gastric emptying in normal subjects—a reproducible technique using a single scintillation camera and computer system. Gut 24, 1117–1125.

Crowley, K.J., Zografi, G., 2003. The effect of low concentrations of molecularly dispersed poly(vinylpyrrolidone) on indomethacin crystallization from the amorphous state. Pharm. Res. 20, 1417–1422.

Han, Y.-J., Stucky, G.D., Butler, A., 1999. Mesoporous silicate sequestration and release of proteins. J. Am. Chem. Soc. 121, 9897–9898.

Hancock, B.C., 2002. Disordered drug delivery: destiny, dynamics and the Deborah number. J. Pharm. Pharmacol. 54, 737–746.

Hancock, B.C., Parks, M., 2000. What is the true solubility advantage for amorphous pharmaceuticals? Pharm. Res. 17, 397–404.

Heikkilä, T., Salonen, J., Tuura, J., Hamdy, M.S., Mul, G., Kumar, N., Salmi, T., Murzin, D.Y., Laitinen, L., Kaukonen, A.M., Hirvonen, J., Lehto, V.-P., 2007a. Mesoporous silica material TUD-1 as a drug delivery system. Int. J. Pharm. 331, 133–138.

Heikkilä, T., Salonen, J., Tuura, J., Kumar, N., Salmi, T., Murzin, D.Y., Hamdy, M.S., Mul, G., Laitinen, L., Kaukonen, A.M., Hirvonen, J., Lehto, V.-P., 2007b. Evaluation of mesoporous TCPSi, MCM-41, SBA-15, and TUD-1 materials as API carriers for oral drug delivery. Drug Deliv. 14, 337–347.

Heikkilä, T., Santos, H.A., Kumar, N., Murzin, D.Y., Salonen, J., Laaksonen, T., Peltonen, L., Hirvonen, J., Lehto, V.P., 2010. Cytotoxicity study of ordered mesoporous silica MCM-41 and SBA-15 microparticles on Caco-2 cells. Eur. J. Pharm. Biopharm. 74, 483–494.

Heinz, A., Savolainen, M., Rades, T., Strachan, C.J., 2007. Quantifying ternary mixtures of different solid-state forms of indomethacin by Raman and near-infrared spectroscopy. Eur. J. Pharm. Sci. 32, 182–192.

Hess, S., Teubert, U., Ortwein, J., Eger, K., 2001. Profiling indomethacin impurities using high-performance liquid chromatography and nuclear magnetic resonance. Eur. J. Pharm. Sci. 14, 301–311.

Horcajada, P., Rámila, A., Pérez-Pariente, J., Vallet-Regí, M., 2004. Influence of pore size of MCM-41 matrices on drug delivery rate. Micropor. Mesopor. Mater. 68, 105–109.

Imaizumi, H., Nambu, N., Nagai, T., 1980. Stability and several physical properties of amorphous and crystalline forms of indomethacin. Chem. Pharm. Bull. 28, 2565–2569.

Kaneniwa, N., Otsuka, M., Hayashi, T., 1985. Physicochemical characterization of indomethacin polymorphs and the transformation kinetics in ethanol. Chem. Pharm. Bull. 33, 3447–3455.

Kim, H.J., Ahn, J.E., Haam, S., Shul, Y.G., Song, S.Y., Tatsumi, T., 2006. Synthesis and characterization of mesoporous Fe/SiO$_2$ for magnetic drug targeting. J. Mater. Chem. 16, 1617–1621.

Kozlova, S.A., Kirik, S.D., 2010. Post-synthetic activation of silanol covering in the mesostructured silicate materials MSM-41 and SBA-15. Micropor. Mesopor. Mater. 133, 124–133.

Kresge, C.T., Leonowicz, M.E., Roth, W.J., Vartuli, J.C., Beck, J.S., 1992. Ordered mesoporous molecular sieves synthesized by a liquid-crystal template mechanism. Nature 359, 710–712.

Legendre, B., Feutelais, Y., 2004. Polymorphic and thermodynamic study of indomethacin. J. Therm. Anal. Calorim. 76, 255–264.

Li, M., Conrad, B., Maus, R.G., Pitzenberger, S.M., Subramanian, R., Fang, X., Kinzer, J.A., Perpall, H.J., 2005. A novel oxidative degradation pathway of indomethacin under the stressing by hydrogen peroxide. Tetrahedron Lett. 46, 3533–3536.

Limnell, T., Santos, H.A., Mäkilä, E., Heikkilä, T., Salonen, J., Murzin, D.Y., Kumar, N., Laaksonen, T., Peltonen, L., Hirvonen, J., 2011. Drug delivery formulations of ordered and nonordered mesoporous silica: Comparison of three drug loading methods. J. Pharm. Sci., doi:10.1002/jps.22577.

Mellaerts, R., Mols, R., Jammaer, J.A.G., Aerts, C.A., Annaert, P., Van Humbeeck, J., Van den Mooter, G., Augustijns, P., Martens, J.A., 2008. Increasing the oral bioavailability of the poorly water soluble drug itraconazole with ordered mesoporous silica. Eur. J. Pharm. Biopharm. 69, 223–230.

Mellaerts, R., Houthoofd, K., Elen, K., Chen, H., Van Speybroeck, M., Van Humbeeck, J., Augustijns, P., Mullens, J., Van den Mooter, G., Martens, J.A., 2010. Aging behavior of pharmaceutical formulations of itraconazole on SBA-15 ordered mesoporous silica carrier material. Micropor. Mesopor. Mater. 130, 154–161.

Nováková, L., Matysová, L., Havlíková, L., Solich, P., 2005. Development and validation of HPLC method for determination of indomethacin and its two degradation products in topical gel. J. Pharm. Biomed. Anal. 37, 899–905.

Nunes, C.D., Vaz, P.D., Fernandes, A.C., Ferreira, P., Romão, C.C., Calhorda, M.J., 2007. Loading and delivery of sertraline using inorganic micro and mesoporous materials. Eur. J. Pharm. Biopharm. 66, 357–365.

Patterson, J.E., James, M.B., Forster, A.H., Lancaster, R.W., Butler, J.M., Rades, T., 2005. The influence of thermal and mechanical preparative techniques on the amorphous state of four poorly soluble compounds. J. Pharm. Sci. 94, 1998–2012.

Qu, F., Zhu, G., Huang, S., Li, S., Sun, J., Zhang, D., Qiu, S., 2006. Controlled release of Captopril by regulating the pore size and morphology of ordered mesoporous silica. Micropor. Mesopor. Mater. 92, 1–9.

Salonen, J., Laitinen, L., Kaukonen, A.M., Tuura, J., Björkqvist, M., Heikkilä, T., Vähä-Heikkilä, K., Hirvonen, J., Lehto, V.P., 2005. Mesoporous silicon microparticles for oral drug delivery: loading and release of five model drugs. J. Control. Release 108, 362–374.

Savolainen, M., Kogermann, K., Heinz, A., Aaltonen, J., Peltonen, L., Strachan, C., Yliruusi, J., 2009. Better understanding of dissolution behaviour of amorphous drugs by in situ solid-state analysis using Raman spectroscopy. Eur. J. Pharm. Biopharm. 71, 71–79.

Shen, S.C., Ng, W.K., Chia, L., Dong, Y.C., Tan, R.B.H., 2010. Stabilized amorphous state of ibuprofen by co-spray drying with mesoporous SBA-15 to enhance dissolution properties. J. Pharm. Sci. 99, 1997–2007.

Shenderovich, I.G., Buntkowsky, G., Schreiber, A., Gedat, E., Sharif, S., Albrecht, J., Golubev, N.S., Findenegg, G.H., Limbach, H.-H., 2003. Pyridine-15 N a mobile NMR sensor for surface acidity and surface defects of mesoporous silica. J. Phys. Chem. B 107, 11924–11939.

Sing, K.S.W., Everett, D.H., Haul, R.A.W., Moscou, L., Pierotti, R.A., Rouquerol, J., Siemieniewska, T., 1985. Reporting physisorption data for gas/solid systems with special reference to the determination of surface area and porosity. Pure Appl. Chem. 57, 603–619.

Song, S.-W., Hidajat, K., Kawi, S., 2005. Functionalized SBA-15 materials as carriers for controlled drug delivery: influence of surface properties on matrix–drug interactions. Langmuir 21, 9568–9575.

Suwalski, A., Dabboue, H., Delalande, A., Bensamoun, S.F., Canon, F., Midoux, P., Saillant, G., Klatzmann, D., Salvetat, J.P., Pichon, C., 2010. Accelerated Achilles tendon healing by PDGF gene delivery with mesoporous silica nanoparticles. Biomaterials 31, 5237–5245.

Vallet-Regí, M., Rámila, A., del Real, R.P., Pérez-Pariente, J., 2001. A new property of MCM-41: drug delivery system. Chem. Mater. 13, 308–311.

Vallet-Regí, M., 2006. Ordered mesoporous materials in the context of drug delivery systems and bone tissue engineering. Chem. Eur. J. 12, 5934–5943.

Van Speybroeck, M., Barillaro, V., Thi, T.D., Mellaerts, R., Martens, J., Van Humbeeck, J., Vermant, J., Annaert, P., Van den Mooter, G., Augustijns, P., 2009. Ordered mesoporous silica material SBA-15: A broad-spectrum formulation platform for poorly soluble drugs. J. Pharm. Sci. 98, 2648–2658.

Wang, F., Hui, H., Barnes, T.J., Barnett, C., Prestidge, C.A., 2010. Oxidized mesoporous silicon microparticles for improved oral delivery of poorly soluble drugs. Mol. Pharmaceutics 7, 227–236.

Watanabe, T., Wakiyama, N., Usui, F., Ikeda, M., Isobe, T., Senna, M., 2001. Stability of amorphous indomethacin compounded with silica. Int. J. Pharm. 226, 81–91.

Yoshioka, M., Hancock, B.C., Zografi, G., 1994. Crystallization of indomethacin from the amorphous state below and above its glass transition temperature. J. Pharm. Sci. 83, 1700–1705.

Zhao, D., Feng, J., Huo, Q., Melosh, N., Fredrickson, G.H., Chmelka, B.F., Stucky, G.D., 1998a. Triblock copolymer syntheses of mesoporous silica with periodic 50 to 300 Ångstrom pores. Science 279, 548–552.

Zhao, D., Huo, Q., Feng, J., Chmelka, B.F., Stucky, G.D., 1998b. Nonionic triblock and star diblock copolymer and oligomeric surfactant syntheses of highly ordered, hydrothermally stable, mesoporous silica structures. J. Am. Chem. Soc. 120, 6024–6036.

Zhao, X.S., Lu, G.Q., Whittaker, A.K., Millar, G.J., Zhu, H.Y., 1997. Comprehensive study of surface chemistry of MCM-41 using 29Si CP/MAS NMR, FTIR, pyridine-TPD, and TGA. J. Phys. Chem. B 101, 6525–6531.